



WE-NEED

WatEr NEEDs, availability, quality and sustainability



Deliverable Number:	D3.3a
Work package number:	WP3
Deliverable title	TRANSPORT EXPERIMENTS INCLUDING MODELING AND ANALYSIS
Type	Report
Dissemination Level	Public
Lead participant	Weizmann Institute of Science
Contributing scientists and other personnel	Brian Berkowitz, Ishai Dror, Natalia Goykhman, Yinon Yechezkel, Jayashree Nath
Scheduled delivery date	30 April 2018
Actual / forecast delivery date	15 April 2018

Deliverable summary

This deliverable summarizes first transport experiments and their analysis, investigating transport and fate of representative emerging contaminants (ECs): silver nanoparticles (Ag-NPs), and the pharmaceutically-active substances oxaliplatin, carboplatin and azithromycin. A more complete analysis is expected in Deliverable 3.3b, to follow in about six months. Analytical protocols to detect the presence and concentration of these ECs are based on methods developed and reported in previously submitted Deliverables. The report systematic transport experiments including mass balance results and analysis. The complex matrices include soils and soil solutions from a field site in Israel. The report includes detailed protocols for the experimental set-ups, in both fully and partially saturated porous media. These methods are being used as the foundation for associated deliverables that are related to the study of transport, fate and risk assessment of these compounds in the environment, at the field scale.

D3.3a

Transport experiments including modeling and analysis

1. Introduction	3
2. Complex matrices of this study	3
2.1 Soil matrices and soil solutions - composition and properties.....	3
2.2 Experimental set-ups	6
3. Quantification of ECs in complex matrices.....	12
3.1 Quantification of pharmaceutically active substances in soil and soil solution.....	12
3.2 Quantification of ENPs in soil and soil solution	17
4. References.....	29

1. Introduction

This deliverable summarizes first transport experiments and their analysis, investigating transport and fate of representative emerging contaminants (ECs): silver nanoparticles (Ag-NPs), and the pharmaceutically-active substances oxaliplatin, carboplatin and azithromycin. A more complete analysis is expected in Deliverable 3.3b, to follow in about six months. Analytical protocols to detect the presence and concentration of these ECs are based on methods developed and reported in previously submitted Deliverables. The report systematic transport experiments including mass balance results and analysis. The complex matrices include soils and soil solutions from a field site in Israel. The report includes detailed protocols for the experimental set-ups, in both fully and partially saturated porous media. These methods are being used as the foundation for associated deliverables that are related to the study of transport, fate and risk assessment of these compounds in the environment, at the field scale.

Abbreviations appearing in the text: **BTC** – breakthrough curve; **CEC** – cation exchange capacity; **DDW** – double distilled water; **EC** – emerging contaminant; **ENP** – engineered nanoparticle; **ICP-MS** – inductively coupled plasma – mass spectrometer; **MW** – molecular weight; **(E)NP** – (engineered) nanoparticle; **PV** – pore volume; **EPV** – effective pore volume

2. Complex matrices of this study

2.1 Soil matrices and soil solutions - composition and properties

2.1.1 Characterization of soil from Weizmann Institute campus, Israel - Soil was collected from the upper 5 cm of the soil layer and for all experiments, the soil was sieved (60 mesh). The basic chemical properties of the soil are provided in Table 1. Weizmann soil is rich in sand and silt and relatively poor in clay. Thus most of the soil particles have relatively small surface area, which might decrease the retention and the number of the possible interactions of the introduced ECs.

Quartz sand (30/40 mesh = 420–600 μm) was used as a benchmark (purchased from Unimin Corporation). Prior to use it was washed in 1% HCl and dried at 105 °C.

Table 1. Weizmann Institute soil characteristics.

Properties	Methods	Weizmann Soil
Composition		89% \pm 3% sand 7% \pm 4% silt 3% \pm 1% clay
pH	DDW	7.97 \pm 0.01
	DDW+CaCl ₂	7.41 \pm 0.02
Porosity		0.39 \pm 0.03


Organic matter (%)		0.5% ± 0.2%
CEC composition [meq/100g]	Na ⁺	0.27
	K ⁺	0.13
	Mg ²⁺	1.21
	Ca ²⁺	8.71
Total CEC [meq/100g]		10.32
Inorganic carbon [%]	CO ₃ -C, %	0.14 ± 0.02
Dissolved Organic Carbon [ppm]	UV at 254 nm	1.00 ± 0.06
Fe [μgr/gr _{soil}]	Acid Extraction	64±7






The carbonate content of the soil is relatively low (which decreases soil buffering capacity), while the cation exchange capacity (CEC) is relatively high (which promotes soil redox buffering). The soil is also very poor in organic matter, which implies a lower amount of possible interactions, as well as lower redox buffering. Therefore the overall pH and redox buffering effects are difficult to predict.

2.1.2 Aquifer porous media from Emilia Romagna, Italy - The aquifer material samples were collected from cores (220-S10 and 221-S6) drilled in 2016 in the Emilia Romagna, Italy. Core 220 S10 comes from a depth of 70 m. It was drilled starting from the bottom of a quarry (about 14 m below ground level). The core essentially contains coarse-grained deposits (gravel and sand) characterizing aquifer A1 in this portion of the alluvial fan, ending within clayey sediments that separate A1 from the underlying aquifer A2.

Each sample was taken from the core at different depths with the aim of characterizing the observable lithological facies. Samples n° 1 to n°4 from 220-S10 and samples n°5 and 6 come from borehole 221-S6. A more detailed characterization of each sample is given in Table 2 based on visual observation and gathering data. No information is available regarding the sand/silt/clay content, pH values, organic carbon content, organic matter content, nitrogen content, C/N ratio, or cation exchange capacity.

Table 2. Soil sample characteristics.

Sample	Core	Depth from ground [m]	Sample weight [g]	Geological Description	
1	220-S10	51.8-52	1129.09	The sample is mainly formed by sand (fluvial channel sands) with very few pebbles (maximum length 2 cm)	(1) 

2	220-S10	48.4-48.6	1049.64	Sandy silt with some pebbles	(2) 
3	220-S10	35.3-35.5	1486.84	Fluvial channel gravel. Heterometric gravel with grain size ranging from fine gravel (about 2 mm – the most abundant fraction) to pebbles (2-3 cm), in sandy-silt matrix	(3) 
4	220-S10	24.5-24.7	1195.89	Clay and silt of alluvial plain. Fine grained material (silt)	(4) 
5	221-S6	8.3-8.6	1184.95	reddish sand	(5) 
6	221-S6	15.6-16	1214.07	clay	(6) 

2.1.3 Handling and preparation of aquifer material samples from Emilia Romagna, Italy -

As can be seen from the pictures in Table 2 the samples are characterized by rocky structures and occurrence of large aggregates. Usually, disaggregation should be performed with minimal force, so the original texture of the soil will be changed as little as possible. In this case, it was necessary to use anvil and hammer to process each sample to an acceptable size. The samples are sieved (mesh size 18-60 mesh) as recommended from ISO standard on soil sampling (ISO 10381-6), thus obtaining a good homogenization. Before each experiment, the soils are air-dried at ambient temperature (preferably between 20-25 °C), weighed and then placed in the oven at 105 °C (approx. 12 hours) to enable calculation of the content of dry mass [%].

2.2 Experimental set-ups

2.2.1 Column experiments for fully saturated conditions - This setup was applied mostly for experiments with soil from Weizmann campus, Israel. The soil was packed into vertical polycarbonate columns, and fully saturated with water by a peristaltic pump from the bottom of the column (Figure 1).

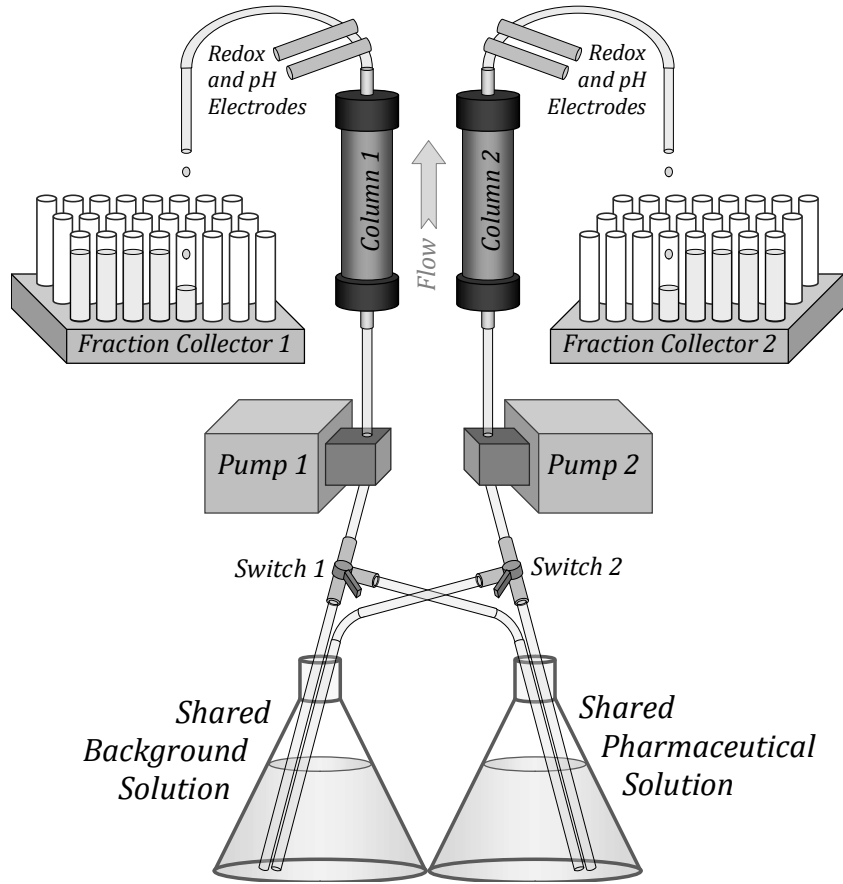


Figure 1. The experimental setup: two packed polycarbonate columns (L×D: 20 cm × 3.2 cm), fed simultaneously from the same inlet solution, connected to two automatic fraction collectors. The columns are covered in aluminum foil to prevent photochemistry. Eh and pH electrodes are attached to the columns outlet and the respective measurements are logged automatically every 10 to 12 minutes.

The soil was not sterilized to allow for induced development of different redox conditions in the experiment. Following saturation, the desired redox conditions were achieved in the column by flushing it with the appropriate synthetic water solution. The experiments were conducted under the following redox conditions: oxic ($pe+pH = 16.6-20.9$), nitrate reducing ($pe+pH = 12.5-14.2$), iron reducing ($pe+pH = 6.5-10.2$), and methanogenic conditions ($pe+pH = 5.6-3.9$). The redox conditions were chosen according to their

potential to affect pharmaceutical transport in soil-water environments, and cover most of the range of natural redox conditions present in aquifer systems [1-7]. Oxidic experiments were also carried out in quartz sand. Other oxidic experiments in sand were carried out with chelating agents (citrate, humic acid and humic acid at buffered pH 9.8) added to the inlet solution composition; these agents differ significantly in size and functionality, are known to complex oxaliplatin or similar materials [8-11], and are likely to be present in wastewaters and the natural environment [12]. In each experiment, two duplicate columns were run simultaneously from the same inlet solution.

To verify that the desired redox condition was established, the redox potential Eh and pH were monitored “on-line” at the outlet of the column (according to Table 3). The synthetic water used in the experiments, to develop specific redox zones, was produced according to Table 4. The salt concentrations were established according to the literature and several preliminary experiments.

Table 3. Experimental pe+pH regimes.

Regime	pH [avg.]	Eh [V]	pe	pe+pH
Oxidic	9.6	414 - 668	7 - 11.3	16.6 - 20.9
Nitrate reducing	8.3	250 - 350	4.2 - 5.9	12.5 - 14.2
Iron reducing	8.5	(-120) - 120	(-2.0) - 2.0	6.5 - 10.2
Strongly reducing	9.0	(-200) - (-300)	(-3.4) - (-5.1)	5.6 - 3.9

For iron reducing conditions, synthesized goethite was incorporated into the soil (4% by weight; other procedures were attempted unsuccessfully). Sodium acetate and methanol were used as easily degradable organic substrates, i.e., the electron donors in different redox conditions. [Goethite synthesis: 0.25 mol of $\text{FeCl}_2 \cdot 2\text{H}_2\text{O}$ and 0.75 mol of NaOH were dissolved in 1L of DDW (NaOH was added in excess). The solution was vigorously shaken, sealed and either left at 90 °C overnight or left at 24 °C for 48 h (several goethite batches were prepared). After cooling to room temperature, the solution was filtered through 0.45 μm filters (PVDF membrane), washed with diluted HCl, washed with DDW, and air-dried. The goethite structure was verified by XRD.]

Upon stabilization of the desired redox conditions, a solution of the relevant synthetic water, inert tracer (500 ppb of Br^-) and the studied EC was delivered at a constant rate of 1 to 1.1 mL/min. The emerging effluent was collected into polypropylene tubes by a fraction collector and filtered through 0.45 micron filters (PVDF membrane) for further detection. The oxaliplatin pulse lasted for approximately 62 pore volumes (PVs). At the end of the oxaliplatin pulse, the inlet solution was replaced by the background solution and a flushing phase was carried out for approximately 10 PVs.

Table 4. Composition of redox solutions.

Substance	Mw [g/mol]	Oxic		Nitrate Reducing		Iron Reducing		Methanogenic	
		C		C		C		C	
		mmol/L	ppm	mmol/L	ppm	mmol/L	ppm	mmol/L	ppm
MgSO ₄ •7H ₂ O	246.47	0.63	157	0.63	157	0.63	157	0.63	157
K ₂ HPO ₄	174.17	0.02	4	0.02	4	0.02	4	0.02	4
NaHCO ₃	84.01	0.27	23	0.27	23	0.27	23	0.27	23
CaCl ₂	110.98	1.14	127	1.14	127	1.14	127	1.14	127
NH ₄ Cl	53.50	0.10	6	0.10	6	0.10	6	0.10	6
KNO ₃	101.10	0.10	10	0.69	70	0.10	10	0.10	10
KBr	119	0.004	0.5	0.004	0.5	0.004	0.5	0.004	0.5
NaCH ₃ COO	82.03	0.73	60	0.73	60	0.73	60	1.10	900
MeOH	32.04	31	10 ml/L	31	10 ml/L	31	10 ml/L	31	10ml/L
Ionic Strength [mmol/L]		8.3		8.9		8.3		8.7	
Na ₃ C ₆ H ₅ O ₇ •2H ₂ O	294.10	0.006	1.78	---		---		---	
Ionic Strength [mmol/L]		8.3		---		---		---	
Purified Humic Acid	2,000-500,000		10-13.5	---		---		---	
Goethite		---		---		4.3% w/w		---	
Oxaliplatin	397.29	0.002	0.6	0.002	0.6	0.002	0.6	0.002	0.6

Metal-based species (oxaliplatin and carboplatin) and bromides were detected by Inductively Coupled Plasma Mass Spectrometer (ICP-MS) (Agilent 7700s). Prior to measurement, collected fractions were acidified to a final concentration of ~2% HNO₃, in all cases, except for the experiments with humic acid. The retardation factor R_f was calculated as $R_f = (PV_{50\%Pt}) / (PV_{50\%Br-})$, i.e., the PV at which Pt recovery is 50% of its plateau value (where the relative concentration stabilizes at a maximum value) divided by the PV at which bromide recovery is 50% of its plateau value. At the end of column experiments, soil was extracted from the column and divided into slices for further detection of oxaliplatin and mass balance calculations, aimed to determine the spatial distribution (along column length).

The experimental results were modeled based on the Hydrus 1D modeling environment [13]. Modeling of the experimental data provides estimates of the types of sorption reactions (instantaneous vs. kinetic), the rates of the kinetic sorption, and the value of the partition coefficient K_d that serves as an indicator for affinity to the matrix surface.

Analysis of carboplatin - Carboplatin transport experiments and detection will follow the same procedure as for oxaliplatin. So far, carboplatin was studied in quartz sand under oxic conditions, and under oxic and methanogenic conditions.

Analysis of azithromycin - Azithromycin is a broad spectrum antimicrobial agent that is approved for use in humans. Due to azithromycin's low rate of metabolism it is likely to be found in wastewater treatment plants, where its broad spectrum of antimicrobial activity could lead to development of resistance in bacteria. The most commonly and suitably used technique for determination of azithromycin in pharmaceutical dosage forms is liquid chromatography-mass spectrometry (LC-MS). A mobile phase containing 70:30:0.1 % of Acetonitrile:Methanol:Formic acid gives best elution of Azithromycin and its common metabolites such as 9-N-desmethylazithromycin, Declandose and N-desmethylazithromycin.

2.2.2 Column experiments for partially saturated conditions - This setup was applied mostly for experiments with sand and soil from Weizmann campus, Israel. The soil was packed into vertical polycarbonate columns, and fully saturated with water by a peristaltic pump from the bottom of the column. Transport experiments were performed by injecting ENP solutions into the column inlets and continuously analyzing ENP concentrations in the column outlets. These measurements were used to determine and interpret breakthrough curves (BTC) (effluent concentration vs. time or volume of applied solution).

Partially saturated conditions were achieved by controlling a pressure difference along the columns; the outlets of the columns were located in a low-pressure chamber while their inlets were exposed to atmospheric pressure (Figure 2). The pressure gradient, controlled by a valve and monitored by a digital vacuum meter, enabled solution flow through the columns under partial saturation. Measurements of water content at the end of each experiment were used to estimate the column saturation. In general, all transport experiments were run in triplicates, using three separate columns simultaneously and applying the same ENP suspension, wash solution, multichannel pump and pressure conditions.

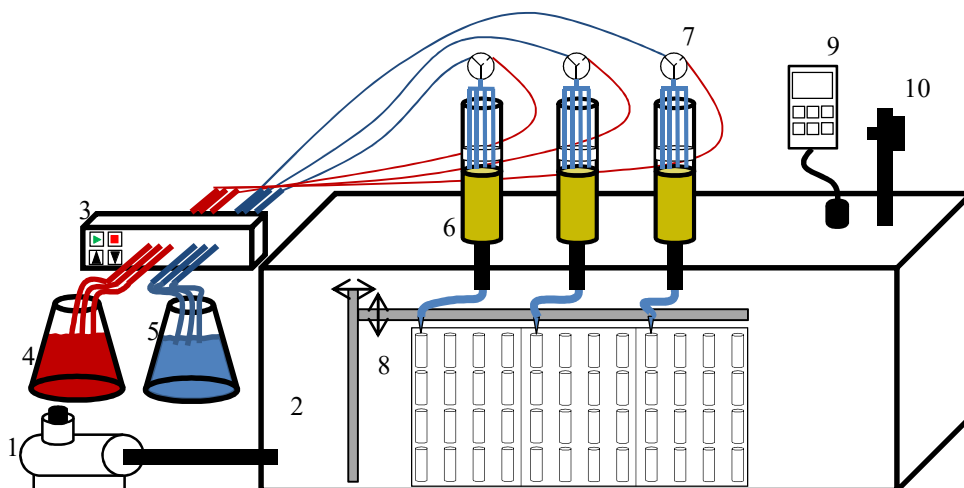


Figure 2. Schematic illustration of the experimental system: 1) vacuum pump; 2) low pressure chamber; 3) multichannel peristaltic pump; 4) ENP suspension; 5) background solution; 6) cylindrical acrylic glass columns; 7) valve to control inlet source solution; 8) fraction collector consisting of stationary tube trays and moving arms; 9) vacuum meter, and 10) valve to control the pressure inside the chamber.

The transport of Ag-NPs in partially saturated sand columns was studied. Each column was fed by four drip infiltration tips, which were connected to two source-solutions: the ENP suspension and the washing/background solution. A T-valve was used to control the flow between the two sources. To examine the effect of CaCl_2 as background solution on the transport of Ag-NPs, another four tips were added to each column, connected directly to the background solution; and the flow rate per each dripping tip was reduced by 50% to maintain the total flow rate. Ag-NP suspension (100 mg L^{-1}) was synthesized by a citrate reduction method [14, 15]. The stock suspension was filtered through $0.22 \mu\text{m}$ filter to avoid large aggregates, then 2-20 mL of the filtered suspension was diluted in deionized water before use according to each column experiment. The silver ionic content in Ag-NP suspension was evaluated to be less than 2% and the pH of the inlet suspensions was in the range of 7-7.5.

Partially saturated conditions were achieved by controlling a pressure difference along the columns; the column outlets were located in a low-pressure chamber while their inlets were exposed to atmospheric pressure. The pressure gradient, controlled by a valve in the low-pressure (outlet) chamber and monitored by a digital vacuum meter, enabled solution flow through the columns under partial saturation. Gravimetric measures of the dry and wet (before and at the end of each experiment, respectively) columns were used to estimate soil moisture and calculate the volumetric water content. Note that column wetting and partially saturated steady state flow involved, by definition, a preferential flow; however, no wall effect was observed during any part of the experiments. Additionally, the spatial water content along the column depth was found to be nearly

uniform (relative standard deviation <6%) without any noticeable trend (results not shown). To study the influence of saturation level on Ag-NP transport, Ag-NP BTCs were determined from experiments performed at different pressure gradients.

Transport of Ag-NPs was measured in a series of soil column experiments. Each column was fed by eight drip infiltration tips, with four connected to either of two source-solutions: the Ag-NP suspension and the flushing/background solution. A three-way valve controlled flow between the two sources. The other four tips were connected only to the flushing/background solution. The rate of downward flow in each column top (inlet) was constant and controlled by two peristaltic pumps. First, the system was allowed to equilibrate to achieve steady-state flow through the columns; the Ag-NP input step was then applied followed by flushing of the column with Ag-NP free solution. Electrolyte solution influences the Ag-NP surface charge and increases Ag-NP retention. To avoid chemical interference of the background solution, and to emphasize the chemical effect of the soil solution, deionized water was used as the flushing/background solution with two exceptions: 425 mg L⁻¹ (1.8 mM) Ca(NO₃)₂·4H₂O solution was applied to study the in situ effect of Ca²⁺ on Ag-NP transport and retention; and the influence of dissolved organic matter was studied by using 30 mg L⁻¹ humic acid (Sigma Aldrich) in both flushing/background solution and Ag-NP suspension. The ionic strength and major cation composition of the soil pore solutions were measured for representative experiments (procedure and results are given in the ESI†). An ionic strength of 0.7 mM was measured for the soil pore solution when deionized water was used as background solution. The effluents were collected in plastic tubes using a fraction collector, and concentrations were then measured to determine BTCs. To examine the vertical distribution of entrapped Ag-NPs in the column, a retention profile (RP) was determined by sampling directly at the conclusion of an experiment. All experiments were run in triplicates, using three separate columns simultaneously and applying the same Ag-NP suspension, wash solution, multichannel pumps and pressure conditions. A tracer transport was conducted as an independent experiment in the same manner as for the Ag-NPs.

Each BTC experiment involved several steps. First, the column was equilibrated with background solution; solution was supplied for at least 12 h under the same condition as in the next steps, to achieve steady-state flow through the column. In parallel, ENP suspension was circulated in the pumping tubes to equilibrate the tubing and achieve a stable ENP concentration in the column inlet. Then the inlet source was changed from washing solution to ENP suspension, with continuous step input lasting 174 min, followed by return to washing solution for an additional 180 min. The effluents were collected in plastic tubes using a fraction collector, at intervals of 6 min, and analyzed for metal concentration via ICP-MS. At the end of each experiment, the columns were weighed to calculate the water content. To examine the vertical distribution of entrapped

ENPs in the column, a retention profile (RP) was used. RP is defined here as a spatial profile of ENP mass normalized to the total ENP mass retained in the column (%). Each column was divided into 8 segments, and each segment was analyzed for ENP content.

Ag-NP concentrations were measured by inductively coupled plasma - mass spectrometry (ICP-MS, Agilent 7700), and based on a calibration curve of Ag-NP suspensions used in the same experiment and prepared by the same protocols. The samples were treated with thiosulfate-cupric-ammonia mixture to ensure Ag-NP (and possibly other silver precipitate) dissolution, based on a silver leaching method.

To determine the retention profile of nanoparticles in the soil column, the columns were dismantled at the end of each experiment and divided into 8 segments (about 1 cm each); then the wet segments were oven-dried to determine the soil moisture. Subsequently, 20 mL thiosulfate-cupric-ammonia mixture (0.05 M ammonium thiosulfate, 0.125 M ammonium sulfate and 0.5 mM cupric sulfate, the mixture pH was adjusted to ca. 9 using NaOH) was added to each dry soil sample, followed by 24 h shaking. The soil was then separated and the supernatant was analyzed. Extraction efficacy (generally >90%) was determined for each experiment separately and accounted for in yield calculations.

3. Quantification of ECs in complex matrices

3.1 Quantification of pharmaceutically active substances in soil and soil solution

3.1.1 Analysis of oxaliplatin in soil column experiments - Oxaliplatin transport characteristics in sand and soil columns vary markedly as a function of porous medium, and are affected to a lesser extent by the medium redox conditions and cation activity in the inlet solution.

In sand, there was little interaction of oxaliplatin species with the sand surface in the oxic experiment, and the interaction was practically unaffected by addition of citrate to the inlet solution (Figure 3). Humic acid, in contrast, had a larger impact on oxaliplatin transport in sand: ~70% of the inlet oxaliplatin species precipitated with humic acid in the sand column at neutral to acidic pH. This pH-dependent precipitation was reversible, and at pH >8, humic acid-bound oxaliplatin eluted almost unretarded. Overall, oxaliplatin species were hardly retained in sand (at pH >8), with and without added chelators.

In soil, oxaliplatin interaction with the porous medium was significantly stronger, and indicated variability in sorption sites and sorption mechanisms (Figure 4). The results fall into two groups: oxic to sub-oxic conditions (group 1), and anoxic conditions (group 2). In general, as the conditions become less oxic, K_d values increase (indicating stronger affinity to soil), and R_f values decrease (indicating faster interaction). Moreover, in all cases the Hydrus model, which is constrained to the assumption of a linear sorption,

failed to describe accurately the characteristics of the experimental BTCs, indicating that the actual sorption does not follow a linear model.

In group 1, K_d values are relatively low, indicating relatively weak affinity to soil. The reaction with soil is fast, leading to slow transport. In group 2, K_d values are significantly larger than in group 1, indicating strong affinity to soil. Larger K_d values in a reduced soil-water environment are consistent with the findings of Turner et al. [20], who found that oxaliplatin exhibits higher K_d values in oxide free, organics-free sediments than in natural sediment. The reaction rate with soil, and the occupation of sorption sites, is slower.

The strongest retention of oxaliplatin species was achieved under iron reducing conditions, although this depends strongly on the availability and quantity of iron oxides in soil; it is also reversible. Additional insights can be gained by excluding iron reducing conditions from comparison, as the soil composition in the experiment differed from the other experiments. Consequently, there is a clear trend of decreasing affinity to soil as the conditions become less reducing, accompanied by an increase in sorption strength.

To isolate the effect of inlet solution chemistry, oxic and iron reducing conditions (lower cation activity) were also compared separately from nitrate reducing and methanogenic conditions (higher cation activity). At lower cation activity, desorption is weaker. Within the first pair, under iron reducing conditions, oxaliplatin species exhibit stronger affinity to soil (K_d) and stronger sorption than under oxic conditions, probably due to the favorable sorption sites provided by the added goethite species. In contrast, there is no clear trend within the second pair of redox conditions: oxaliplatin species exhibit stronger affinity to soil under methanogenic conditions, but stronger sorption under nitrate reducing conditions. Under methanogenic conditions, some of the soil organic functional groups have undergone reduction, apparently altering some thermodynamically favorable sorption sites to more easily accessible but less binding sites.

Overall, none of the chelators or soil redox conditions induce a sufficient, long term retardation mechanism for oxaliplatin and oxaliplatin-related species. One implication of these findings is that efforts to attenuate oxaliplatin transport in soil-water environments by manipulation of redox or pH regimes will not be sufficient to prevent aquifer system contamination; prevention, reduction, or control of contamination by oxaliplatin and its derivatives may be better achieved by collection and treatment of hospital effluents at source, before they are released to aquifer and soil-water environments.

The initial results of carboplatin transport experiments (figure not shown) differ significantly from the corresponding oxaliplatin experiments, indicating that the structural differences between oxaliplatin and carboplatin indeed induce different interactions with soil-water environment. In both sand and soil, carboplatin species BTCs reach stable plateau, and the recovery is 96 - 98%, indicating very low retention by the

medium surfaces. Yet, the retardation is much stronger in soil, indicating a fast, but easily reversible interaction with soil surface. In soil, the ratio of retained to released species is much lower than in the oxaliplatin case. However, the retardation and retention is stronger under oxic conditions than under methanogenic conditions, as it is in the oxaliplatin case (possibly, following the same reasoning).

The partition coefficient K_d is below 1 (Table 5), indicating very low affinity to both soil and sand, much lower than in the oxaliplatin case. Interestingly, unlike the oxaliplatin case, the K_d is higher for sand than for soil. The modeled graphs fit quite well the experimental result, indicating that the implied linear sorption model is adequate for describing the experimental data.

Overall, the initial results indicate that carboplatin may be quite mobile in a natural soil-water environment, almost unretarded by natural soil surfaces, thus posing a potential risk to water sources contamination.

Table 5. Summary of the calculated transport data and the model-derived parameters K_d in sand and soil experiments of oxaliplatin. The vertical arrows mark the change in direction of values.

		Retained [$\frac{\mu\text{gPt}}{\text{g}_{\text{matrix}} \times \text{PV}}$]	Released [$\frac{\mu\text{gPt}}{\text{g}_{\text{matrix}} \times \text{PV}}$]	Ratio of Retained/ Released	R_f	K_d [mL/g _{matrix}]
Sand	Oxic	0.0075	0.0028	2.7	1.0	2.6
	Citrate	0.0072	0.0042	1.7	1.0	3.5
	Humic acid unbufferd	0.015	0.0084	1.8	0.8	---
	Humic acid buffered	0.0068	0.01	0.7	1.2	0.13
Soil	Oxic	0.14	0.0069	20	2.1	116
	Nitrate reducing	0.11	0.0068	16	2.3	138
	Methanogenic	0.11	0.0082	13	1.7	191
	Iron reducing	0.13	0.0026	50	1.6	642

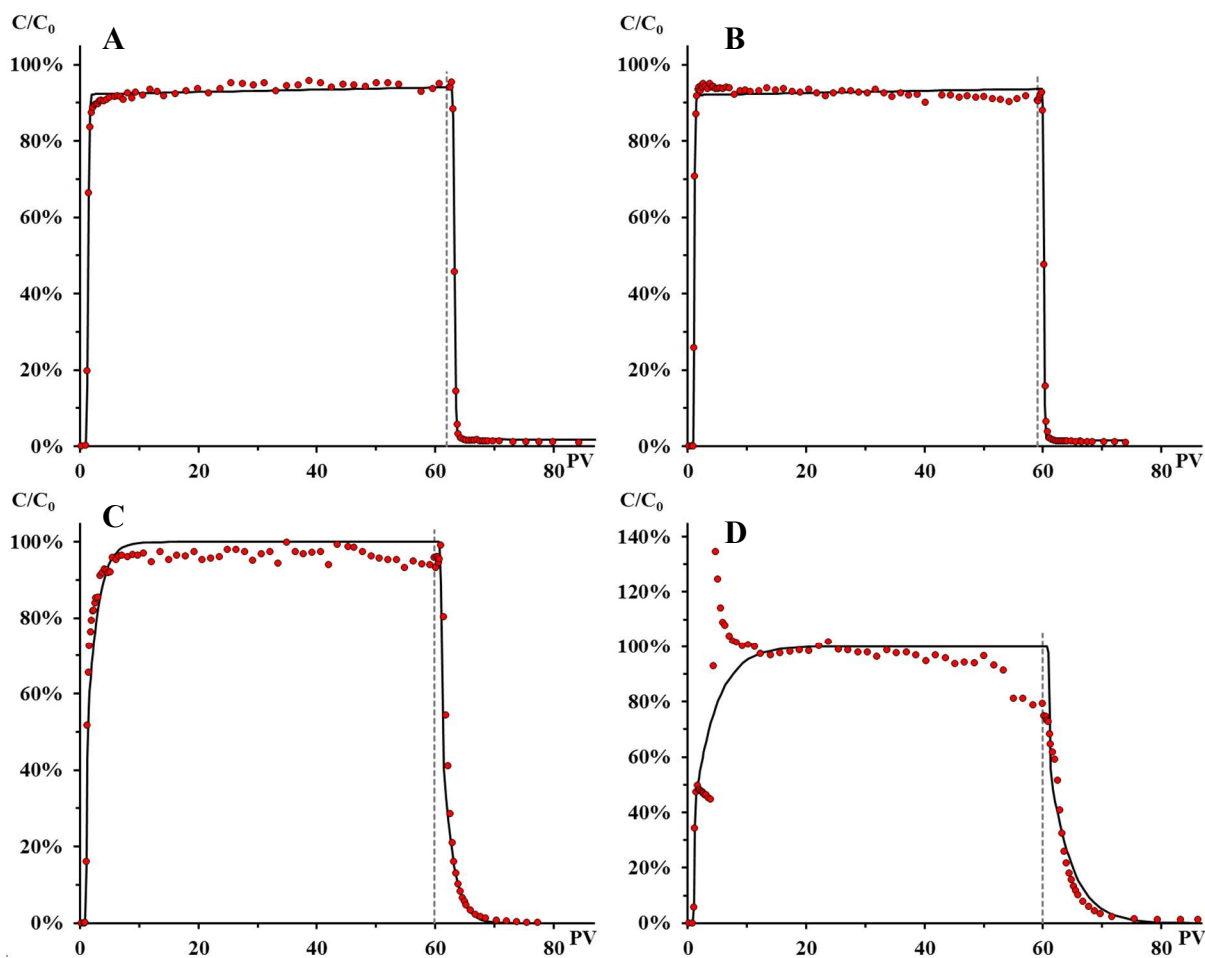


Figure 3. BTCs and model fits of total oxaliplatin species in sand columns. Legend: ● - experimental data, solid line - model, dashed vertical line - start of flushing phase. A. Oxic conditions. B. Oxic conditions with added citrate. C. Oxic conditions with added humic acid at buffered pH 9.8. D. Oxic conditions with added humic acid at unbuffered pH. Note that the scale of the y-axis differs from the scale of graphs A - C.

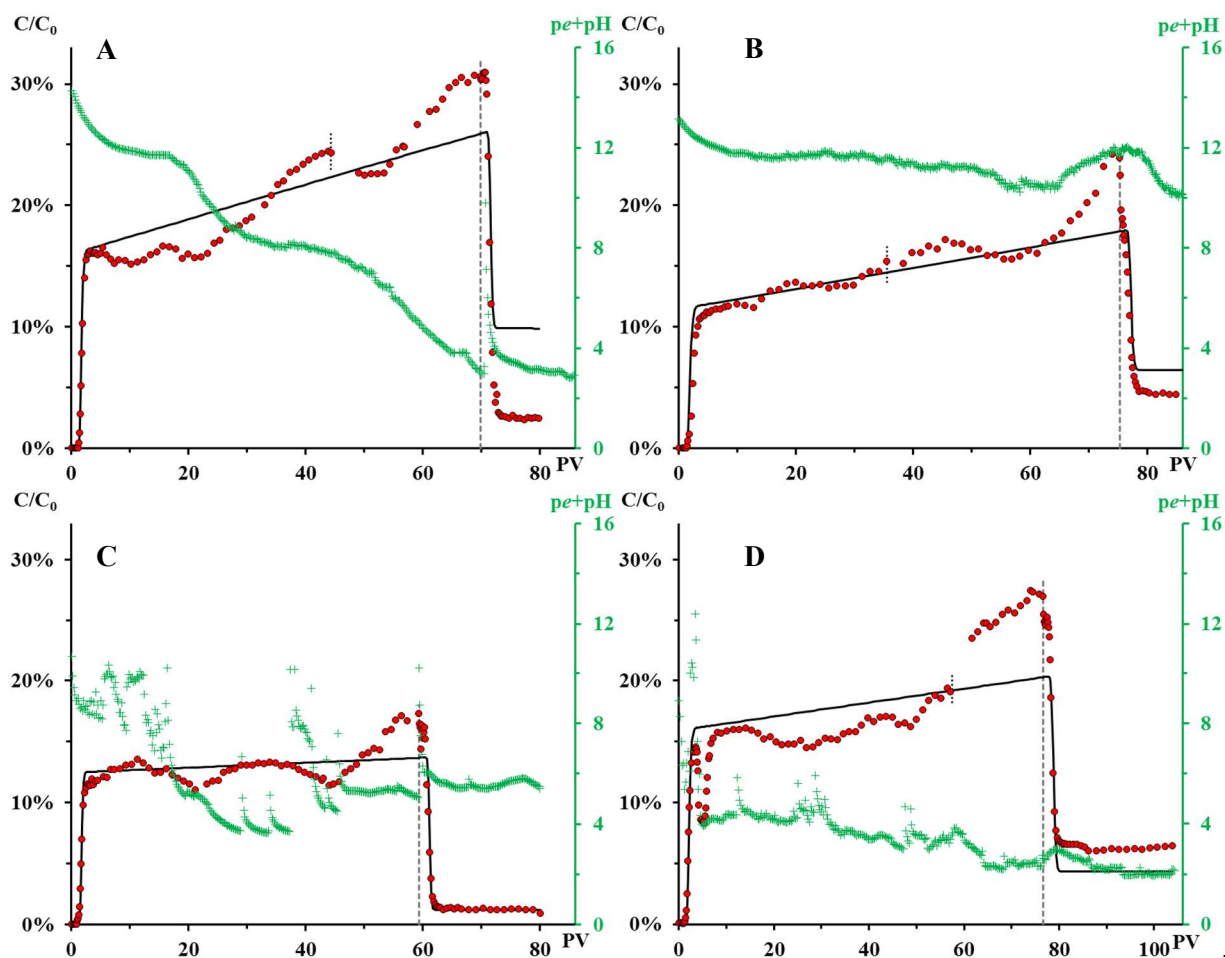


Figure 4. BTCs of total oxaliplatin species in soil (left y-axis), shown together with changes in $pe+pH$ within the soil column as a function of PV (right y-axis). Legend: ● - experimental data, + - $pe+pH$, solid line - model, dashed vertical line - start of flushing phase, short dotted vertical line - change of inlet solution to a freshly prepared one. A. Oxidic conditions. B. Nitrate reducing conditions. C. Iron reducing conditions. D. Methanogenic conditions. Note that the scale of the x-axis is longer than in other soil graphs due to the prolonged duration of the experiment.

3.1.2 Transport of azithromycin and its metabolites in sand/soil - To study the fate and transport of azithromycin in soil-water ecosystems, initial column experiments were designed with sand and aqueous solution of azithromycin at concentration of 1 mg L^{-1} inlet solution. Other parameters for the experiments were maintained at: Flow rate = 1 mL min^{-1} ; pH of initial solution = 6.02; Volume of column = 141.4 mL; Pore Volume (PV) = 40 mL. Azithromycin was injected into the column for 15 PV, followed by washing with DDW for another 7 PV. The sand in the column was divided into 8 fractions and azithromycin was extracted with methanol (overnight shaking at room temperature) (Figure 5). Azithromycin and its metabolites could not be detected over the background level in the column outlet.

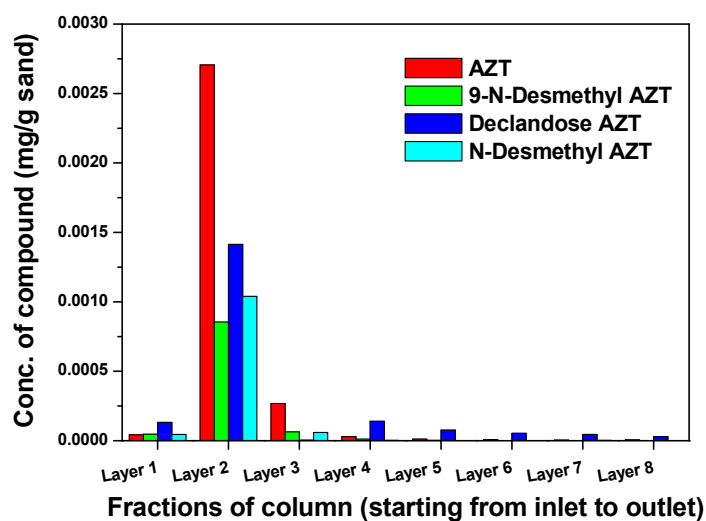


Figure 5. Concentration of azithromycin and its metabolites in fractions of sand column.

3.2 Quantification of ENPs in soil and soil solution

3.2.1 Ag-NP transport and retention - Figure 6 shows Ag-NP transport in a partially saturated soil column, in comparison to Ag-NP transport in a partially saturated sand column, and to bromide (conservative) tracer transport in a partially saturated soil column. A recent study of ENP transport in partially saturated porous media reported tracer-like behavior of Ag-NP transport through sand columns [14]. The current study reveals significant differences between sand and soil with respect to Ag-NP transport. These differences may originate from the different solution chemistry. In particular, the ionic strength and cationic composition of sand and soil pore solutions were significantly different. Higher cation concentrations, mainly divalent cations, which were observed in the soil pore water, increased Ag-NP retention in soil relative to sand. Moreover, differences between Ag-NP transport in soil and sand may be a result of the mineral composition and roughness of soil (and the presence of clay minerals), as compared to sand, as well as to differences in pore and grain sizes of the host porous media.

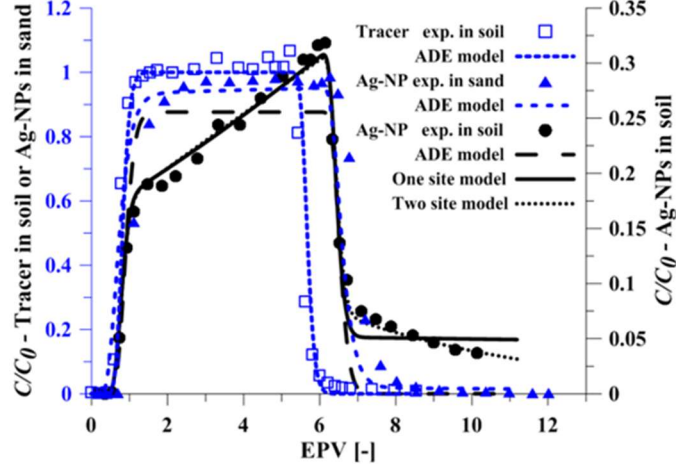


Figure 6. Breakthrough curves of Ag-NPs in partially saturated systems, measurements (dots) and fitted models (lines); bromide tracer in soil (squares) and Ag-NPs in sand (triangles) are related to the left axis, while Ag-NPs in soil (circles) are related to the right axis. One representative experiment of the three replicates is shown here.

Tracer transport in partially saturated soil follows classical advection-dispersion equation (ADE) behavior with negligible retention coefficient (k_{a2}), similar to tracer transport in saturated soil or partially saturated sand [14]. The BTC pattern and plateau (C/C_0) of Ag-NP transport in sand resembles tracer behavior (Figure 6); the ADE model with a small retention coefficient (k_{a2}) describes well the experimental BTC. In contrast, Ag-NP transport in partially saturated soil displays different behavior. In general, the BTC consists of three steps (Figure 6): (1) sharp increase in the relative concentration which appears between 0.5-1 EPV (effective pore volume, defined as the water content of the column under steady-state, partially saturated flow); (2) moderate rise in Ag-NP concentration from about 1-6 EPV (end of Ag-NP pulse); and (3) drop in the effluent Ag-NP concentration, with a long BTC tail.

Hydrus 1D is a computer software package widely used to model water and heat flow and transport of multiple solutes in variably saturated porous media [13]. Here, the inverse mode of Hydrus 1D was applied to fit model parameters to experimental BTC results, using a nonlinear least squares optimization routine. A two-site kinetic model with attachment/detachment retention mechanisms was applied. The two-site model accounts for Ag-NP retention on two types of attachment sites, each governed by independent attachment and detachment rates, a different total number of sites, and different retention mechanisms. The two types of attachment sites are referred to here as site 1 and site 2. The mass balance for this application is based on a modified form of the advection-dispersion equation (ADE) given by

$$\frac{\partial(\theta C)}{\partial t} - \rho \frac{\partial S_1}{\partial t} - \rho \frac{\partial S_2}{\partial t} = \frac{\partial}{\partial z} \left(\theta D \frac{\partial C}{\partial z} \right) - \frac{\partial(qC)}{\partial z} \quad (1)$$

where θ is the volumetric water content, C [ng mL⁻¹], S_1 and S_2 [ng g⁻¹] are the Ag-NP concentrations in the aqueous and solid phases (retained on sites 1 and 2), respectively, ρ is the soil bulk density [g cm⁻³], t is time [min], z is the distance from column inlet [cm], D is the hydrodynamic dispersion coefficient [cm² min⁻¹] and q is the water flux [cm min⁻¹]; θ was measured at the end of each column experiment and assumed to be constant given that the experiment reached steady-state flow. The dispersivity is determined by fitting tracer experiments to the conventional ADE model. For attachment/detachment retention, the terms for solid phase mass balance can be replaced by

$$\rho \frac{\partial S_1}{\partial t} = \theta k_{a1} \psi C - k_{d1} \rho S_1 \quad (2)$$

$$\rho \frac{\partial S_2}{\partial t} = \theta k_{a2} C - k_{d2} \rho S_2 \quad (3)$$

where k_{a1} , k_{a2} , k_{d1} and k_{d2} are the first-order attachment and detachment coefficients for sites 1 and 2, respectively [min⁻¹] and ψ is a retention function that determines the nature of the attachment mechanism for the first retention site. Here, ψ is a time-dependent retention function which is related to k_{a1} (site 1):

$$\psi = \left(1 - \frac{S}{S_{max}}\right) \quad (4)$$

where S_{max} is the maximum solid phase concentration on site 1 [ng g⁻¹]. This retention function is based on a Langmuirian type equation and is frequently terms ‘blocking’; it represents a decrease in the attachment rate as the attachment sites are occupied and S approaches S_{max} . Note that for large values of S_{max} , the term is nearly 1 and the attachment rate is constant rather than time-dependent. Time-dependent blocking results in a uniform RP when all deposition sites are occupied. When k_{a2} is set to zero, the system becomes a one-site, time-dependent retention model, while setting k_{a1} to zero reduces the system to the ADE with constant attachment. Zeroing both k_{a1} and k_{a2} returns equation (1) to the classical ADE.

An inverse solution for the two-site model was first applied by fitting four retention parameters (k_{a1} , S_{max} , k_{a2} , k_{d2}) to the experimental BTC data ($R^2 > 0.97$ in all cases); then, when similar fitting values for different experiments were obtained, the number of fitted parameters was reduced by fixing other parameters to an average value, if applicable. To simulate both reversible and irreversible retention mechanisms, the detachment mechanism was considered only for site 2 (k_{d2}); a detachment mechanism is rarely used when the BTC decreases sharply to very low concentrations after a pulse input. However, addition of a detachment mechanism is required to control the gradual decrease in the BTC tail. These attachment and release mechanisms strongly influence the RP pattern and modeling of spatial retention in the column.

The use of a two-site model in this study enables fitting of the BTC tail, separate reversible and irreversible processes, and examination of the relative contribution of each mechanism. We further note that Ag-NP transport in partially saturated soil shows negligible depth-dependency for the experimental results (RP pattern), which is corroborated by a two-site model simulation (comparing retention on time-dependent sites to retention on depth-dependent sites; results not shown). Therefore, a depth-dependent retention function is not incorporated here.

An additional important difference between Ag-NP BTC patterns in soil and sand is related to the BTC tail during the flushing stage (Figure 6). The Ag-NP concentration in sand drops rapidly to very low values following the end of the Ag-NP pulse; this behavior resembles a tracer BTC pattern (Figure 6); similar tailing behavior has been shown previously for Ag-NP transport in saturated sand and soil. Partially saturated soil columns lead to different behavior compared to partially saturated sand or saturated systems. Figure 6 shows longer tailing for Ag-NP transport in partially saturated soil, with an initial sharp drop in Ag-NP concentration (in this case from $C/C_0 = \sim 0.35$ to ~ 0.07), followed by a gradual decrease during the flushing phase. This pattern indicates that Ag-NPs are released and remobilized after the Ag-NP pulse ends. Consequently, a detachment mechanism, which is frequently ignored or neglected, should be considered in this case.

To examine the effect of input concentration, transport and retention experiments were examined for four Ag-NP input concentrations: 94, 576, 889 and 1820 ng mL⁻¹. As input concentration increases, the BTC slope (step 2) becomes steeper (Figure 7), and higher C/C_0 values of step 1 are observed. However, the BTC shape is different at the highest input concentration (1820 ng mL⁻¹) and discussed below. The change in BTC slope can be explained by the increase in the input concentration, where the time-dependency increases due to faster occupation of attachment sites. Nevertheless, the increase in step 1 value (Figures 7a-c) is not explained by the different input concentrations. From examination of the model parameters, a change in attachment coefficient(s) will lead to alteration of the initial breakthrough.

Repulsion interactions between Ag-NPs can reduce the attachment coefficient by impeding further attachment of Ag-NPs on sites that already been partially occupied. Thus, higher input concentration results in more NPs being attached to the matrix, which in turn decreases k_{a2} . Experiments 1-3 show that the fitted parameters support this observation: a decrease in k_{a2} was found for the first three concentrations while the other parameters were similar and therefore fixed to identical values.

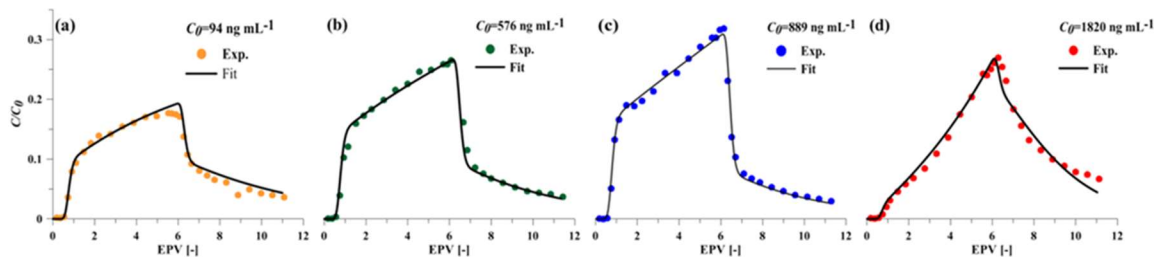


Figure 7. Breakthrough curves (BTCs) of Ag-NP transport in partially saturated soil columns for input concentrations (C_0 , in ng mL^{-1}) (a) 94, (b) 576, (c) 889, and (d) 1820. Experimental data (symbols) and fitted models (lines) are given as relative concentration, C/C_0 . One representative experiment of the three replicates is shown here.

Characterization of the aggregation state, in the presence of soil solution, as a function of Ag-NP concentration reveals formation of larger aggregates at relatively high Ag-NP concentration (2000 ng mL^{-1}), in contrast to lower concentrations (Figure 8). These results are consistent with measurements of Klitzke et al. [16], who showed minimal aggregation of Ag-NPs at a concentration of 500 ng mL^{-1} and much faster formation of substantially larger aggregates at concentrations of $5,000$ and $10,000 \text{ ng mL}^{-1}$. The collision efficiency between Ag-NPs increases with particle concentration, which results in increased aggregation; at lower Ag-NP concentrations, the probability for NPs to collide and thus aggregate is thus lower. This process may be enhanced in soil solutions, where the diffusive double layer is compressed due to the presence of divalent and trivalent cations [16]. Despite the occurrence of aggregation at high Ag-NP concentrations, the zeta potentials of Ag-NPs and aggregates are similar. Therefore, the obtained aggregates may be considered as larger colloids, which are not NPs by definition, but have similar composition and surface charge characteristics.

The BTC in Figure 7d is different in all three steps, when compared to Figures 7a-c. The initial breakthrough (step 1) is hardly noticeable, which is related to increases in k_{a1} and k_{a2} ; the steeper slope in step 2 is explained by high time-dependency that results from high input concentration; and the larger angle of the BTC tail (step 3) originates from considerable Ag-NP release (an increased detachment coefficient). For experiment 4, the experimental observations and model parameters both indicate that a different retention mechanism becomes dominant. Increases in k_{a2} , k_{d2} and k_{a1} values were found for the fourth Ag-NP input concentration, compared to a decrease in only one parameter (k_{a2}) for the three lower concentrations. These results imply that different retention mechanisms occur and govern Ag-NP aggregate transport, and indicate nanospecific transport behavior when comparing Ag-NPs to colloids of the same material. For this case, we suggest the occurrence of induced straining due to aggregation. Both film straining and pore straining are minimal for nanosized particles and become relevant for larger aggregates, which may explain the increase in the values of the attachment coefficients and the change in the detachment rate.

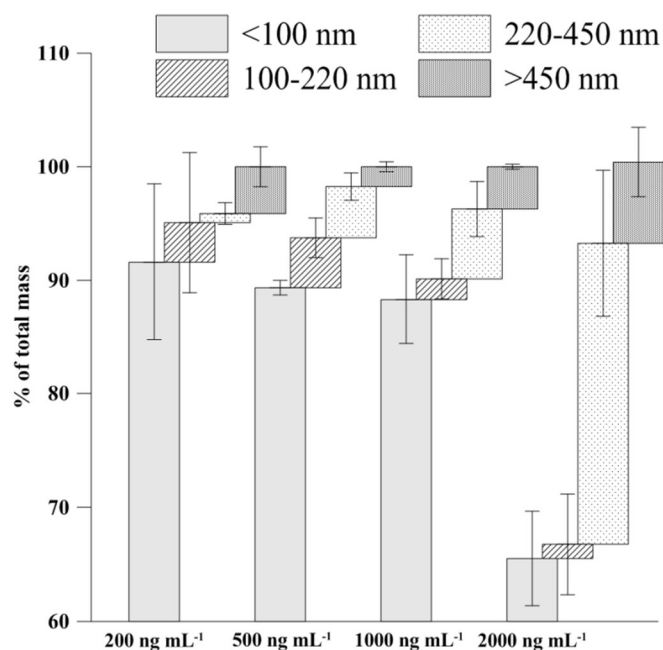


Figure 8. Aggregation state of Ag-NPs. Size fractions of <100, 100-220, 220-450 and above 450 nm are presented for AgNPs at different concentrations (200-2000 ng mL⁻¹) suspended in soil solution. Error bars indicated standard deviation of three replicates.

The Ag-NP retention and mobility change with input concentration (Figure 7). Nanospecific transport is observed at low concentrations, with no change in the retention mechanism. The time dependency and initial retention rate are determined directly by the concentration, while the attachment rate on site 2 is the only model parameter being affected. Once the Ag-NP concentration increases above a threshold value, significant aggregation leads to additional retention mechanism(s) – possibly including straining of aggregates – which affect(s) the retention and release rates on both sites.

The effect of water content (water saturation level) on Ag-NP transport was studied by comparing three similar experiments at $\theta=0.28, 0.35$ and 0.38 . The BTCs given in Figure 9a show an increase in Ag-NP mobility with water saturation. Note that Ag-NP pulse duration, indicated by cross symbols in Figure 9a, decreases from 5.5 to 3.9 EPVs with increasing water content. Therefore, differences on the horizontal axis are due to different EPV values in each experiment. The eluted phase recovery grows from 29.1% to 39% and 51.8% for saturation levels of 73%, 92% and >99%, respectively. The BTC patterns also indicate different behavior of Ag-NPs in saturated and partially saturated soil. In the fully saturated column, a plateau is reached immediately following step 1, reducing the

slope in step 2 to almost zero. This pattern indicates low time-dependency; as suggested from equation (4), the time-dependency is minimized when S_{max} is extremely high ($\psi=1$) or extremely low ($\psi=0$). Indeed, the saturated BTC can be well modelled by both high and low values of S_{max} (not shown). A high S_{max} value is assumed to enhance Ag-NP retention unless compensated by a low attachment coefficient; however, the observed BTC shows higher mobility. In addition, a lower S_{max} value was fitted for higher water saturation in the case of experiments 3 and 5, while a one-site model with constant attachment rate (equations (1-4), with $S_{max} \rightarrow 0$ thus $\psi=0$), was applied in experiment 6. Although the three curves show different step 1 and 2 shapes, they converge to a similar BTC tail pattern in step 3.

A possible explanation for the tailing behavior is a different attachment rate related to site 1, but similar attachment and release rates for site 2. In this case the explanation links the time-dependent retention to the saturation level, which further implies that attachment on site 1 is related to the AWI (air-water interfaces) or air-solid-water interfaces. This also means that attachment and release from site 2 are independent of water saturation. Attachment of ENPs to AWI was reported previously: Chen et al. [17] showed an approximately linear proportion between TiO_2 NP retention (in glass beads) and AWI area for saturation levels higher than 40%. Adsorption of TiO_2 NPs to the AWI was therefore suggested to be the primary retention mechanism at high saturation. Kumahor et al. [18] reported reversible, equilibrium attachment of Ag-NPs to the AWI in a sand column experiment, but suggested that the reversibility of attachment is sensitive to solution chemistry.

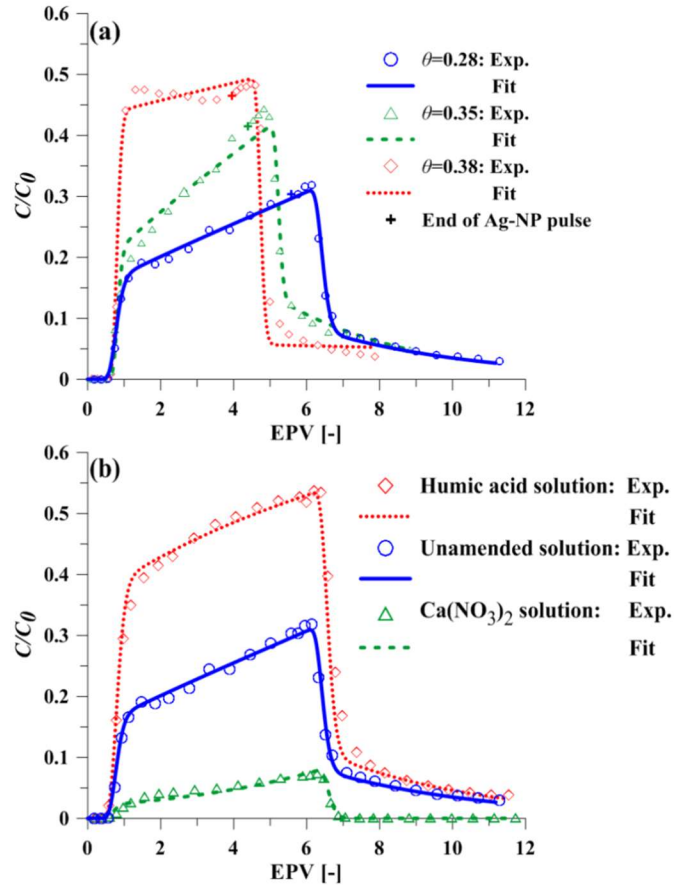


Figure 9. Ag-NP transport (a) at different water content levels; and (b) in the presence of humic acid (30 mg L⁻¹), Ca(NO₃)₂ (425 mg L⁻¹) and unamended solution. Symbols indicate experimental data; lines refer to model results. Note that Ag-NP pulse duration, indicated by the cross symbol, decreases from 5.5, to 4.4, and then to 3.9 EPVs with increasing water content. One representative experiment of the three replicates is shown here.

An additional retention mechanism that should be considered in partially saturated flow is film straining. However, the efficiency of film straining decreases with increasing saturation level and increases with colloid size, hence its contribution to Ag-NP (diameter approx. 40 nm) retention at saturation levels >70% is not significant. The fitted parameters for the lower saturation experiments show a decrease in k_{a1} and S_{max} with increasing saturation (experiments 3 and 5). (It can be noted, parenthetically, that because hydraulic parameters (such as porosity, flux and water content) affect retention parameters (such as k_a , k_d and S_{max}), comparison of model solutions wherein only one parameter is varied does not necessarily reflect actual BTC behavior. For example, the result shown in Fig. 2f, wherein only the water content parameter is modified, indicates increased Ag-NP retention with increasing water content, in contrast to the actual measurements; in this case, S_{max} would be expected to change with an increase in the water content.) Attachment on the air-water interface is suggested to be related to the time-dependent retention of Ag-NPs in partially saturated soil; note that other time-dependent mechanisms may also exist. This retention explains only part of the total retained mass; the remaining mass retained in the column is suggested to be independent of the saturation level.

Ag-NPs may interact with the soil solution, which affects their stability in the solution and therefore their transport behavior. Moreover, interactions of Ag-NPs with the soil solution may also affect NP-collector interactions by, for example, bridging between NPs and soil, altering electrostatic interactions (by divalent cations), or increasing steric effects by organic matter. Many studies reported that electrolyte solutions affect ENP transport [19,20]. Furthermore, changes in solution chemistry may affect ENP retention by altering the number of attachment sites [19]. Here we examine the effect of humic acid (ubiquitous in natural soil-water environments) as an Ag-NP stabilizer, and the effect of $\text{Ca}(\text{NO}_3)_2$ solution (abundant in soil environments) on Ag-NP transport. Figure 9b presents BTCs of experiments 3, 7 and 8. A significant increase in Ag-NP mobility is observed in the presence of humic acid, while significant retention was found in the presence of $\text{Ca}(\text{NO}_3)_2$, compared to the unamended solution. The retained mass recoveries were 47.9%, 71.4% and 95.3% for humic acid solution, unamended solution, and $\text{Ca}(\text{NO}_3)_2$ solution, respectively.

Humic acid improves Ag-NP stabilization by coating the Ag-NPs, thus increasing steric effects, preventing Ag-NP aggregation and reducing their interaction with solution components and possibly with the solid phase (a slight reduction in Ag-NP zeta potential was found). As a consequence, a decrease in attachment rates k_{a1} and k_{a2} is expected (experiments 3 and 7). The presence of humic acid did not affect the BTC slope, compared to unamended solution, which implies similar S_{max} , k_{d2} and C_0 values (parameters affecting the BTC slope). Moreover, the value of S_{max} is related to the saturation level, which remained similar in these experiments. Therefore, in the model simulations, S_{max} and k_{d2} values were fixed to the same fitted values as for the unamended solution (experiments 3 and 7). It is noted here that altering both S_{max} and k_{d2} in such a way that the BTC slope remains similar to that for unamended solution contradicts the known effect of humic acid and is therefore not appropriate.

In the presence of $\text{Ca}(\text{NO}_3)_2$ solution, the BTC demonstrates high retention and low mobility with $C/C_0 < 0.06$. The BTC sharply decreased to low concentrations immediately after the Ag-NP pulse, which indicates an insignificant release of attached Ag-NPs. Indeed, the model parameter optimization returns a negligible k_{d2} value when the two-site model was applied (not shown), and therefore a one-site, time-dependent model is used (experiment 8).

In summary, chemical interactions between Ag-NPs and the soil solution significantly affect (enhancing or suppressing) Ag-NP mobility, by changing the mechanism of retention.

3.2.2 Analysis of Retention Profiles

Figure 10 presents the observed and model corresponding RPs of experiments 1-8. Note that model calculations for the RPs were obtained with the parameters used to fit the BTCs; RP measurements were not employed in a fitting procedure and used to provide a rough qualitative comparison for the simulations. Most of the RPs display uniform or linear decreases (experiments 1-3, 5; Figures 10a,b; $R^2=0.74-0.97$). When the conditions were more favourable for Ag-NP mobility (saturation >99% and in the presence of humic acid) the RPs are nonmonotonic (experiments 6, 7; Figures 10b,c; $R^2=0.06-0.35$). When Ag-NPs were strongly retained in the column (in the presence of $\text{Ca}(\text{NO}_3)_2$ and high input concentration), the RPs are somewhat similar to a hyperexponential pattern (experiments 4, 8; Figures 10a,c; $R^2=0.72-0.79$).

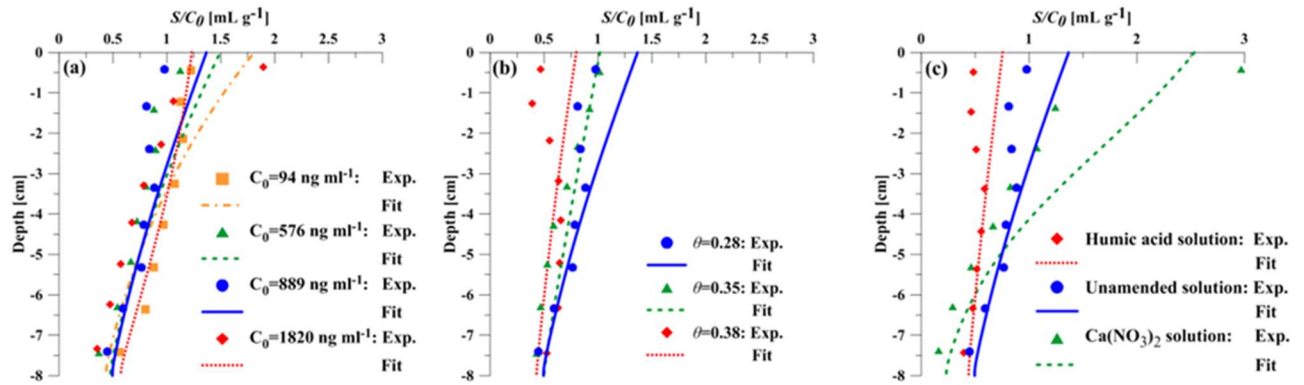


Figure 10. Retention profiles (RPs) of Ag-NP transport in partially saturated soil columns for various input concentration (a), various water contents (b) and in the presence of humic acid (30 mg L⁻¹) and $\text{Ca}(\text{NO}_3)_2$ (425 mg L⁻¹) (c). Experimental data (symbols) and fitted models (lines) are given as S/C_0 (while S is the Ag-NP solid phase concentration [ng g⁻¹] and C_0 is the Ag-NP input concentration [ng mL⁻¹]). Note that RP model results are obtained using parameter values obtained to fit the BTCs; RP measurements were not employed in fitting procedure. One representative experiment of the three replicates is shown here.

In most cases, the observed RPs decreased almost linearly with column depth; similar observations were reported previously,¹⁴ but the retention mechanism(s) leading to such behavior is/are not clearly known.³⁴ Depth-dependent retention is characterized by an hyperexponential pattern that is only weakly evident for the case of experiments 4 and 8 (Figures 10a,c), where significantly higher retention is observed close to the column inlet. Previous studies which employed one- or two-site kinetic models to simulate transport of colloids and ENPs in saturated/unsaturated sand or soil were able to simultaneously match both BTCs and RPs only when an hyperexponential pattern was observed and practically no colloid release was observed [21, 22]. Other studies showed an inability to match the RPs [18, 22, 23]. Wang et al. [24] applied a two-species model to simulate hyperexponential and nonmonotonic RPs of PVP-coated Ag-NPs in saturated soil. It therefore appears that their model cannot provide reliable insights into the

mechanisms controlling ENP transport, particularly in heterogeneous porous media such as soils, due to the large number of fitted parameters ($n \geq 6$).

We note that the observed RPs are a result of both attachment and detachment processes. The spatial (re)distribution of Ag-NPs occurs partially during the column washing step, and is subject to the washing solution wherein the chemical solution may cause ENP release from attachment sites. Therefore, the Ag-NP release process (or efficiency) that applies during the first part of the experiment may be different than the last washing step. In addition, the attachment rate is also subject to change as the Ag-NP concentration in the soil solution decreases with the progress of the washing step.

Amitay-Rosen et al. [25] employed MRI to visualize spatial porosity changes during transport of colloids in porous media. They also observed increases in colloid accumulation with depth (as opposed to the hyperexponential RP pattern), indicating that particles travel some distance with the liquid phase until they are deposited by physicochemical interactions. Here, Ag-NPs are not expected to alter the macroscopic properties of the soil, although such changes should be considered for long-term, concentrated systems with potential Ag-NP aggregation.

We further note that Goldberg et al. [26] assessed several models for ENP transport and concluded that for most cases, model performance should be analysed separately for RPs and BTCs. They point out, too, that none of these models can reproduce a linearly decreasing RP. The model presented in this study provides only a moderate fit to the observed RP, with an average R^2 value of 0.65 (range: $0.06 < R^2 < 0.97$) where the lower R^2 values were obtained for nonmonotonic RPs. This attachment/detachment model is incapable of simulating both Ag-NP BTCs and RPs in partially saturated soil. An additional mechanism that controls the spatial Ag-NP distribution is thus needed to simulate the RP. Hence the model does not offer strong predictive capabilities, but it provides insights into Ag-NP transport mechanisms.

In summary, the transport and retention of citrate stabilized Ag-NPs in partially saturated soil exhibit different patterns when comparing sand and soil, and saturated and partially saturated, conditions. Different retention mechanisms were indicated for each case. In addition, the experiments demonstrated nanospecific transport behavior of Ag-NPs in partially saturated soil, as compared to associated colloids (aggregates). Ag-NP mobility increases with input concentration, which may be related to a decrease in the attachment rate due to repulsion between Ag-NPs. Straining is less likely to occur during Ag-NP transport due to the small ratio between Ag-NP size to soil grain size. Additionally, straining is related to depth-dependent retention which in general was not observed in the RPs. However, straining and depth-dependent retention of Ag-NP aggregates occur when conditions are favorable for induced aggregation, such as high Ag-NP input concentration and presence of Ca^{2+} in solution. Predicted environmental concentrations are not

expected to exceed 1000 ng mL^{-1} ; thus, significant aggregation due to high concentrations is less relevant for most environmental cases. On the other hand, aggregation due to calcium bridging is extremely likely in soil-water environments.

Time-dependent retention of Ag-NPs was found to be related to the saturation level and attachment on the air-water interface. Model analysis indicates a decreasing number of attachment sites with increasing saturation, consistent with the expected decrease in air-water interface area. A fully saturated column experiment shows almost no time-dependency.

Higher mobility was also observed in the presence of humic acid, which prevents the aggregation and interaction of Ag-NPs with soil grains. Lower retention in this case may also be a result of competitive attachment between humic acid and Ag-NPs. However, the presence of humic acid shows no effect on the time-dependency, which may indicate no competitive attachment onto the time-dependent site, but onto other sites.

The BTC tailing shape indicates that Ag-NPs can be released and remobilized upon washing of the column with nanoparticle-free solution. The processes of Ag-NP release may include disaggregation and detachment from secondary minima (more likely) or primary minima (less likely), due to changes in the soil solution chemistry. The release rate and remobilization properties determine Ag-NP spatial distributions (i.e. RPs) which were observed at the completion of each experiment.

4. References

1. Menahem A, *Transport behavior of pharmaceuticals and personal care products in saturated soil under various redox conditions*, M.Sc. thesis, Department of Earth and Planetary Sciences 2014, Weizmann Institute of Science. p. 51.
2. Barbieri M, et al., *Formation of diclofenac and sulfamethoxazole reversible transformation products in aquifer material under denitrifying conditions: batch experiments*. Science of The Total Environment, 2012. 426:p. 256-263.
3. Nodler K, et al., *Evidence for the microbially mediated abiotic formation of reversible and non-reversible sulfamethoxazole transformation products during denitrification*. Water Research, 2012. 46(7):p. 2131-2139.
4. Smith EJ, Davison W, Hamilton-Taylor J, *Methods for preparing synthetic freshwaters*. Water Research, 2002. 36(5):p. 1286-1296.
5. Goeppert N, Dror I, Berkowitz B, *Detection, fate and transport of estrogen family hormones in soil*. Chemosphere, 2014. 95:p. 336-345.
6. Scheytt T, et al., *Transport of pharmaceutically active compounds in saturated laboratory columns*. Ground Water, 2004. 42(5):p. 767-773.
7. Chefetz B, Mualem Y, Ben-Ari J, *Sorption and mobility of pharmaceutical compounds in soil irrigated with reclaimed wastewater*. Chemosphere, 2008. 73(8):p. 1335-1343.
8. Luo FR, Yen TY, Wyrick SD, Chaney SG, *High-performance liquid chromatographic separation of the biotransformation products of oxaliplatin*. Journal of Chromatography B: Biomedical Sciences and Applications, 1999. 724:p. 345-356.
9. Lustig S, Zang S, Beck W, Schramel P, *Dissolution of metallic platinum as water soluble species by naturally occurring complexing agents*. Microchimica Acta, 1998. 129:p. 189-194. 10.1007/BF01244740.
10. Lustig S, Zang S, Michalke B, Schramel P, Beck W, *Transformation behaviour of different platinum compounds in a clay-like humic soil: speciation investigations*. Science of the Total Environment, 1996. 188:p. 195-204.
11. Sures B, Zimmermann S, *Impact of humic substances on the aqueous solubility, uptake and bioaccumulation of platinum, palladium and rhodium in exposure studies with Dreissena polymorpha*. Environmental Pollution, 2007. 146:p. 444-451.
12. Essington ME, *Soil and Water Chemistry: An Integrative Approach*. Taylor & Francis, 2003.
13. Šimůnek J, van Genuchten MT, *Modeling nonequilibrium flow and transport processes using HYDRUS*. Vadose Zone Journal, 2008. 7:p. 782-797.
14. Yechezkel Y, Dror I, Berkowitz B, *Transport of engineered nanoparticles in partially saturated sand columns*. Journal of Hazardous Materials, 2016. 311:p. 254-262.
15. Dong X, Ji X, Wu H, Zhao L, Li J, Yang W, *Shape control of silver nanoparticles by stepwise citrate reduction*, Journal of Physical Chemistry C, 2009. 113:p. 6573-6576.

16. Klitzke S, Metreveli G, Peters A, Schaumann GE, Lang F, *The fate of silver nanoparticles in soil solution — Sorption of solutes and aggregation*, Science of the Total Environment, 2015. 535:p. 54-60.
17. Chen L, Sabatini DA, Kibbey TCG, *Role of the air–water interface in the retention of TiO₂ nanoparticles in porous media during primary drainage*, Environmental Science and Technology, 2008. 42:p. 1916-1921.
18. Kumahor SK, Hron P, Metreveli G, Schaumann GE, Vogel HJ, *Transport of citrate-coated silver nanoparticles in unsaturated sand*, Science of the Total Environment, 2015. 535:p. 113-121.
19. Liang Y, Bradford SA, Šimůnek J, Vereecken H, Klumpp E, *Sensitivity of the transport and retention of stabilized silver nanoparticles to physicochemical factors*, Water Research, 2013. 47:p. 2572-2582.
20. Liang Y, Bradford SA, Šimůnek J, Heggen M, Vereecken H, Klumpp E, *Retention and remobilization of stabilized silver nanoparticles in an undisturbed loamy sandy soil*, Environmental Science and Technology, 2013. 47:p. 12229-12237.
21. Kasel D, Bradford SA, Šimůnek J, Heggen M, Vereecken H, Klumpp E, *Transport and retention of multi-walled carbon nanotubes in saturated porous media: Effects of input concentration and grain size*, Water Research, 2013. 47:p. 933-944.
22. Zhang M, Engelhardt I, Šimůnek J, Bradford SA, Kasel D, Berns AE, Vereecken H, Klumpp E, *Co-transport of chlordecone and sulfadiazine in the presence of functionalized multi-walled carbon nanotubes in soils*, Environmental Pollution, 2017. 221:p. 470-479.
22. Braun A, Klumpp E, Azzam R, Neukum C, *Transport and deposition of stabilized engineered silver nanoparticles in water saturated loamy sand and silty loam*, Science of the Total Environment, 2015. 535:p. 102-112.
23. Wang D, Jaisi DP, Yan J, Jin Y, Zhou D, *Transport and retention of polyvinylpyrrolidone-coated silver nanoparticles in natural soils*, Vadose Zone Journal, 2015, 14(2).
24. Wang D, Ge L, He J, Zhang W, Jaisi DP, Zhou D, *Hyperexponential and nonmonotonic retention of polyvinylpyrrolidone-coated silver nanoparticles in an Ultisol*, Journal of Contaminant Hydrology, 2014. 164:p. 35-48.
25. Amitay-Rosen T, Cortis A, Berkowitz B, *Magnetic resonance imaging and quantitative analysis of particle deposition in porous media*, Environmental Science and Technology, 2005. 39:p. 7208-7216.
26. Goldberg E, Scheringer M, Bucheli TD, Hungerbühler K, *Critical assessment of models for transport of engineered nanoparticles in saturated porous media*, Environmental Science and Technology, 2014. 48:p. 12732-12741.